

Aggregation Dynamics of Rigid Polyelectrolytes

Anvy Moly Tom,^{1, a)} R. Rajesh,^{1, b)} and Satyavani Vemparala^{1, c)}

The Institute of Mathematical Sciences, C.I.T. Campus, Taramani, Chennai 600113, India

(Dated: 16 May 2018)

Similarly-charged polyelectrolytes are known to attract each other and aggregate into bundles when the charge density of the polymers exceeds a critical value that depends on the valency of the counterions. The dynamics of aggregation of such rigid polyelectrolytes are studied using large scale molecular dynamics simulations. We find that the morphology of the aggregates depends on the value of the charge density of the polymers. For values close to the critical value, the shape of the aggregates is cylindrical with height equal to the length of a single polyelectrolyte chain. However, for larger values of charge, the linear extent of the aggregates increases as more and more polymers aggregate. In both the cases, we show that the number of aggregates decrease with time as power laws with exponents that are not numerically distinguishable from each other, and are independent of charge density of the polymers, valency of the counterions, density, and length of the polyelectrolyte chain. We model the aggregation dynamics using the Smoluchowski coagulation equation with kernels determined from the molecular dynamics simulations, and justify the numerically obtained value of the exponent. Our results suggest that, once counterions condense, effective interactions between polyelectrolyte chains short-ranged and the aggregation of polyelectrolytes is diffusion-limited.

Keywords: Aggregation, polyelectrolytes, dynamical properties

I. INTRODUCTION

Many biologically relevant polymers such as DNA, actin and microtubules, have charged, rigid or semiflexible backbone structures, and may aggregate into bundles in the presence of counterions^{1–6}. The aggregates of such biological polymers play an important role in cell scaffolding and possess superior mechanical properties compared to well known synthetic flexible polymers^{7,8}. More recently, it has been possible to synthesize non-biological polymers with comparable backbone stiffness and the ability of these polymers to aggregate is an important parameter in using them as functional biomimetic materials^{9,10}. With recent studies on various biological phenomena such as DNA packaging, cytoskeletal organization, understanding counterion mediated aggregation of charged polymers becomes very relevant^{11,12}.

The aggregation of rigid polyelectrolyte (PE) chains has been studied extensively via experiments^{1,13–21}, simulations in the presence and absence of salt/solvent^{22–33} and theoretical approaches^{34–42}. While it has been fairly well established that multivalent counterions induce aggregation among the similarly charged PEs, the ability of monovalent counterions to induce a similar aggregation is debated^{14–18,21,24,27,28,30,33–35,43–48}. We recently showed, using molecular dynamics simulations as well as computing potential of mean force, that for high enough charge density along PE backbone, monovalent counterions also induce aggregation⁴⁹. Further, this critical charge density for aggregation was numerically shown to be equal

to the critical charge density for the extended-collapsed transition of a *flexible* polyelectrolyte chain^{49,50}.

While the aspect of attraction between similarly-charged PE chains, typically using coarse-grained bead-spring models, is numerically well-studied in the literature^{23–32}, the dynamics of aggregation of such PE chains is less studied. This is in part due to the computational cost of simulating large number of PE chains with long-ranged Coulomb interactions. Using a hybrid Monte Carlo scheme, and simulating a system with 61 PE chains, it was argued that for intermediate values of the charge density, finite-size PE bundles exist at thermodynamic equilibrium, while further increase of charge density, results in phase separation and precipitation^{25,26}. Using similar parameters, the temporal dependence of the number of clusters of different sizes were obtained in Refs.^{22,23}. The numerical data was modeled by the Smoluchowski coagulation equation which is the basis of classical mean-field model of understanding aggregation kinetics⁵¹, and the number of clusters may be deduced to decrease with time as t^{-1} . However, the coagulation kernel was one for particles with equal masses and sizes. This assumption seems unreasonable as the aggregate sizes become heterogeneous with time. In addition, it is not very clear how parameters such as the valency of the counterions, the charge density of PE chains, or the overall number density of the system, affect the aggregation dynamics.

In this paper, using molecular dynamics (MD) simulations (model and MD details in Sec. II), we demonstrate that the aggregation of similarly charged rigid PEs is independent of linear charge density of the polymer chains (higher than a critical value required for onset of aggregation) and valency of counterions, and that the number of aggregates decrease in time as a power law $t^{-\theta}$ where $\theta = 0.62 \pm 0.07$ (Sec. III A). The coagulation process

^{a)}Electronic mail: anvym@imsc.res.in

^{b)}Electronic mail: rrajesh@imsc.res.in

^{c)}Electronic mail: vani@imsc.res.in

is modeled using Smoluchowski equation with a coagulation kernel determined from the MD simulations and reproduces the numerically obtained value for θ , implying that aggregation is diffusion-limited and primarily driven by short-range interactions (Sec. III B). We find that two merging aggregates approach either perpendicular to each other or in a collinear manner depending on the charge density (Sec. III C). Section IV contains a summary and discussion.

II. METHODS

We consider a system of N_r rigid PE chains. Each PE chain consists of N_m monomers, of charge $+qe$, connected by bonds. The counterions have charge $-Zqe$, where Z is the valency of the counterion. In this paper, we consider $Z = 2, 3$ corresponding to divalent and trivalent counterions respectively. The number of counterions are chosen such that the system is overall charge neutral. The interactions between the particles are described below:

Excluded volume: The excluded volume interaction is modeled by the 6-12 Lennard Jones potential:

$$U_{LJ}(r_{ij}) = 4\epsilon_{ij} \left[\left(\frac{\sigma_{ij}}{r_{ij}} \right)^{12} - \left(\frac{\sigma_{ij}}{r_{ij}} \right)^6 \right], \quad (1)$$

where r_{ij} is the distance between particles i and j , ϵ_{ij} is the minimum of the potential and σ_{ij} is the inter-particle distance at which the potential is zero. Both ϵ_{ij} and σ_{ij} are (in reduced units) set to $\epsilon_{ij} = \epsilon = 1.0$ and $\sigma_{ij} = \sigma = 1.0$ for all pairs of particles. The Lennard Jones potential is chosen to be zero beyond a cut-off distance $r_c = \sigma$, such that the excluded volume interaction between all pairs is purely repulsive.

Coulomb: The electrostatic interaction is

$$U_c(r_{ij}) = \frac{q_i q_j}{4\pi\epsilon_0 r_{ij}}, \quad (2)$$

where q_i and q_j are the charges of i^{th} and j^{th} particle, and ϵ_0 is the permittivity.

Bond stretching: The nearest-neighbor monomers along the PE chains are connected by harmonic springs:

$$U_{bond}(r_{ij}) = \frac{1}{2}k(r_{ij} - b)^2, \quad (3)$$

where k is the spring constant and b is the equilibrium bond length. We set $b = 1.12\sigma$ and $k = 500.0$.

Bond bending: To model rigid PEs, a bond bending potential is introduced between two adjacent bonds:

$$U_\theta(\theta) = k_\theta[1 + \cos\theta], \quad (4)$$

where θ is the angle between the bonds. The strength of this interaction is set to a large value $k_\theta = 1000.0$.

The linear charge density along the PE chain is parameterized by a dimensionless quantity A :

$$A = \frac{q^2 \ell_B}{b}, \quad (5)$$

TABLE I. The different values of valency of counterions (Z), charge density A , PE chain length (N_m), and density used in the MD simulations. Density is expressed in terms of $\rho = 3.8 \times 10^{-4}$. The analyses are performed over 20 initial conditions for each set of parameter values.

Z	A	N_m	Density
3	2.01	30	ρ
	3.57	30	0.75ρ
	3.57	30	ρ
	3.57	30	1.5ρ
	4.52	30	ρ
	5.57	30	ρ
	6.75	30	ρ
	8.03	30	ρ
2	3.57	15	ρ
	3.57	30	ρ
	3.57	60	ρ
	5.58	30	ρ
	14.28	30	ρ

where ℓ_B is the Bjerrum length, the length scale below which electrostatic interactions dominate thermal energy⁵²

$$\ell_B = \frac{e^2}{4\pi\epsilon_0 k_B T}, \quad (6)$$

where k_B is the Boltzmann constant and T is temperature.

All the simulations are performed for $N_r = 100$ PE chains at values of A that are larger than the critical value beyond which the PEs aggregate, as determined in Ref.⁴⁹. A variety of parameters such as A , valency of the counterions, PE chain length and density of the system are varied and the details of the systems simulated are given in Table I. The analyses are performed over 20 initial conditions for each set of parameter values in Table I.

The equations of motion are integrated in time using the molecular dynamics simulation package LAMMPS^{53,54}. The simulations are carried out at constant temperature ($T=1.0$), maintained through a Nosé-Hoover thermostat (coupling constant = 0.1)^{55,56}. The long-ranged Coulomb interactions are evaluated using the particle-particle/particle-mesh (PPPM) technique⁵⁷. The time step for integrating equations of motion is chosen as 0.001. A homogeneous initial state is prepared as follows. N_r non-overlapping PE chains of length N_m are placed in a cubic box with periodic boundary conditions with randomly distributed counterions. The charge density of the PE chains is set to a very small value ($A = 0.22$) which ensures that counterions do not condense onto the PE chains. The system is then evolved to ensure homogeneous distribution of the PE chains and

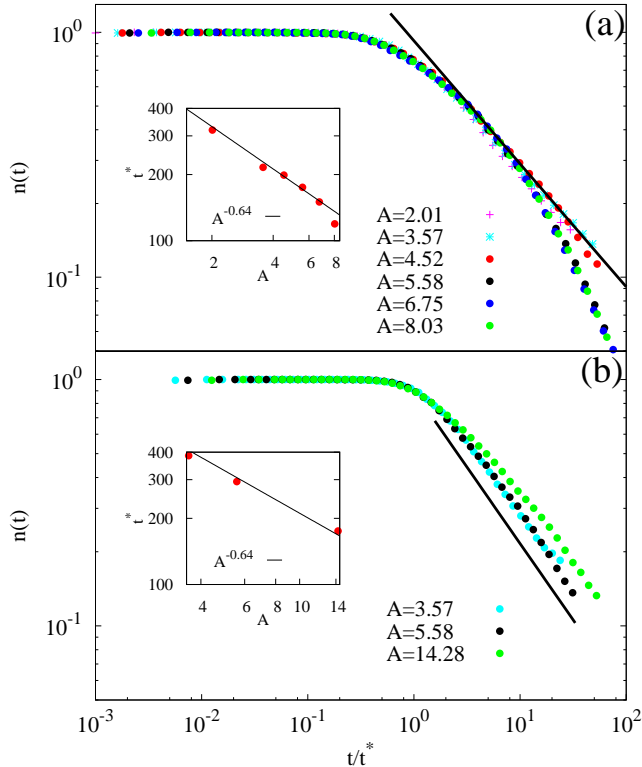


FIG. 1. The variation of the fraction of aggregates $n(t)$ with scaled time t/t^* for different values of A for systems with (a) trivalent and (b) divalent counterions. t^* is the time at which $n = 0.9$. The straight lines are power law $(t/t^*)^{-0.62}$. Inset shows the dependence of t^* on A .

the counterions. Twenty random configurations, which are temporarily well separated, are chosen and appropriate values of A are chosen for further simulations.

III. RESULTS

A. Aggregation Dynamics

We first present results for the temporal dependence of number of aggregates. Two PEs are said to form an aggregate of size two if the distance between any two monomers (not from the same PE) is less than 2σ , and the same definition is extended to an aggregate of size m .

Figure 1(a) and (b) shows the fraction of aggregates $n(t) = N(t)/N(0)$, as a function of time t/t^* for trivalent and divalent counterions respectively. Here, $N(t)$ is the number of aggregates at time t , and t^* is the time taken for number of clusters to reach 90% of $N(0)$. For small times $n(t) \approx 1$ and aggregation is initiated only after t^* , which is the time taken for counterion condensation to occur. Beyond t^* , $n(t)$ decreases as a power law $t^{-\theta}$. From Fig. 1, we find that the exponent θ is independent

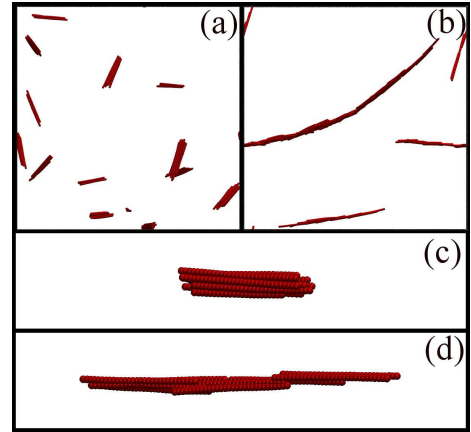


FIG. 2. Snapshots of systems with trivalent counterions for (a) $A = 2.01$ and (b) $A = 8.03$. In (c) and (d), magnified images of clusters of size 10 in the snapshots of (a) and (b) are shown. (Counterions are not shown in the picture for the sake of clarity.)

or utmost very weakly dependent on A as well as valency, and has the value $\theta = 0.62 \pm 0.07$.

For systems with trivalent counterions and large A , we find that $n(t)$ deviates from the power law behavior at long times [see Fig. 1(a)]. To understand this crossover, we study the morphology of the aggregates. Figure 2 shows snapshots of the system for $A = 2.01$ and $A = 8.03$ in (a) and (b), along with enlarged snapshots of aggregates of size 10 in (c) and (d). For smaller values of A , the aggregates are cylindrical in shape with length of the aggregate being roughly the same as the length of a PE, while for larger A , the aggregates are linear but with larger aggregates having longer length. The crossover seen in Fig. 1(a) at long times occurs only for aggregates whose length increases with aggregate size, and is likely a finite size effect due to the size of the aggregate becoming comparable to the system size.

We also confirm that the exponent θ does not depend on the density ρ as well as N_m , the length of the PE chain, as can be seen from the collapse of the data for different ρ and N_m onto one curve [see Fig. 3(a) and (b)]. We thus conclude that the exponent θ characterizing the power law decay of number of aggregates is quite universal and does not appear to depend on parameters such as valency, density or length of the PE. It is thus plausible that aggregation is driven by diffusion and irreversible aggregation (we do not see any fragmentation event) due to short-ranged attractive forces. With this assumption, we recast the aggregation dynamics of PE in terms of the Smoluchowski equation in Sec. III B.

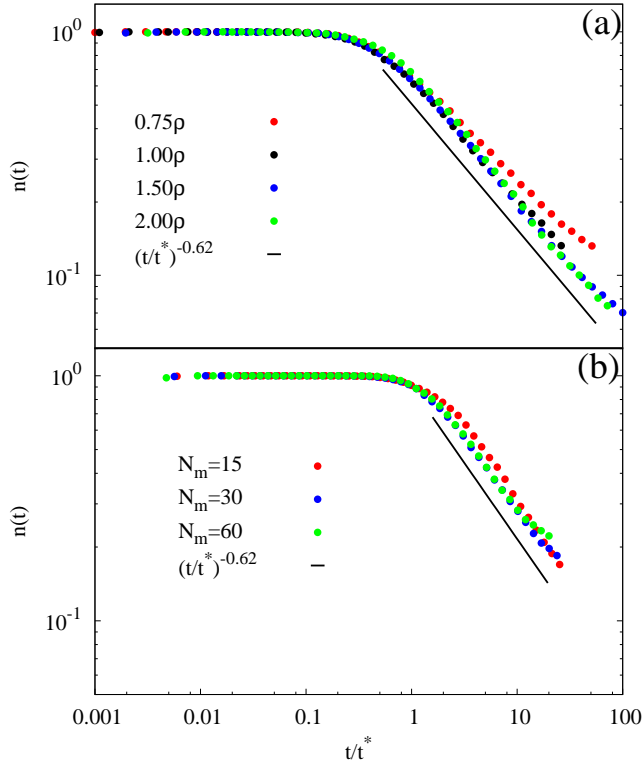


FIG. 3. Fraction of clusters, $n(t)$, as a function of time for (a) different densities and trivalent counter ions, and (b) different PE length N_m and divalent counter ions. The data are for $A = 3.57$.

B. Recasting results in terms of Smoluchowski equation

The Smoluchowski equation describes irreversible aggregation of particles that are transported by some mechanism such as diffusion or ballistic motion. In Sec. III A, we showed that the PE aggregation dynamics is independent of PE charge density (A) and valency of counterions (Z). We model the aggregation as one of diffusing neutral rod-like particles that aggregate due to short-ranged attraction.

The Smoluchowski equation for irreversible aggregation (for reviews, see^{58,59}) is

$$\frac{dN(m,t)}{dt} = \frac{1}{2} \sum_{m_1=1}^{m-1} K(m_1, m-m_1)N(m_1)N(m-m_1) - \sum_{m_1=1}^{\infty} K(m, m_1)N(m)N(m_1), \quad (7)$$

where $N(m,t)$ is the number of aggregates of size m at time t , and $K(m_1, m_2)$ is the rate at which two masses m_1 and m_2 collide. The first term in Eq. (7) describes the aggregation of particles to form an aggregate of size m , while the second term describes the loss of an aggregate of size m due to collision with another aggregate.

If the kernel $K(m_1, m_2)$ is a homogeneous function of its arguments with homogeneity exponent λ , i.e., $K(hm_1, hm_2) = h^\lambda K(m_1, m_2)$, then the number of aggregates $N(t) = \sum_m N(m, t)$, decreases in time as a power law $N(t) \sim t^{-\theta}$, where

$$\theta = \frac{1}{1-\lambda}, \quad \lambda < 1. \quad (8)$$

To construct the kernel $K(m_1, m_2)$, we consider the aggregates to be effective spheres of radius $\sqrt{\ell^2 + r^2}$, where ℓ and r are the height and radius of the cylindrical aggregate. This is justified because we observe that the aggregates rotate at a rate that is much larger than the rate of collision (see Supplementary material) For diffusing spheres in three dimensions, the coagulation kernel is known to be (for example, see⁶⁰)

$$K(m_1, m_2) \propto [D(m_1) + D(m_2)][R(m_1) + R(m_2)], \quad (9)$$

where $D(m)$ and $R(m)$ are the diffusion constant and effective radius of an aggregate of m PEs. In the absence of a solvent, the diffusion constant is inversely proportional to its mass:

$$D(m) \propto m^{-1}. \quad (10)$$

The dependence of the radius $R(m)$ on m may be determined by studying the geometry of the aggregates obtained from the MD simulations. The geometry of an aggregate may be quantified by the eigenvalues of the gyration tensor S whose elements are

$$S_{\alpha\beta} = \frac{1}{N} \sum_{i=1}^N r_{i\alpha} r_{i\beta}, \quad \alpha, \beta = 1, 2, 3, \quad (11)$$

where $r_{i\alpha}$ is the α^{th} component of position vector \vec{r}_i of i^{th} particle measured from the center of mass. Let the eigenvalues be denoted by λ_1, λ_2 , and λ_3 , where $\lambda_1 \geq \lambda_2 \geq \lambda_3$. Modeling the shape of the aggregate as a cylinder, we obtain the length and radius of the aggregate to be $\ell = \sqrt{12\lambda_1}$ and $r = \sqrt{2(\lambda_2 + \lambda_3)}$. The length and radius, thus measured, are shown in Fig. 4 for $A = 2.01$ and $A = 8.03$. For small values of A , ℓ is independent of aggregate size m , i.e. $\ell \sim m^0$, while the radius r increases with m as $r \sim \sqrt{m}$ [see Fig. 4(a)]. For large values of A , we find that $\ell \sim \sqrt{m}$ and $r \sim \sqrt{m}$ [see Fig. 4(b)]. Thus, aggregation is controlled by two types of kernels:

$$\frac{K(m_1, m_2)}{m_1^{-1} + m_2^{-1}} \propto \begin{cases} \sqrt{N_m^2 + m_1} + \sqrt{N_m^2 + m_2} & \text{if } A \gtrsim A_c \\ \sqrt{m_1} + \sqrt{m_2} & \text{if } A \gg A_c, \end{cases} \quad (12)$$

where A_c is the critical charge density beyond which aggregation sets in. The radius and length of cluster are calculated from the eigenvalues of gyration tensor.

For $A \gg A_c$, the kernel is homogeneous with homogeneity exponent $\lambda = -1/2$. From Eq. (8), we obtain

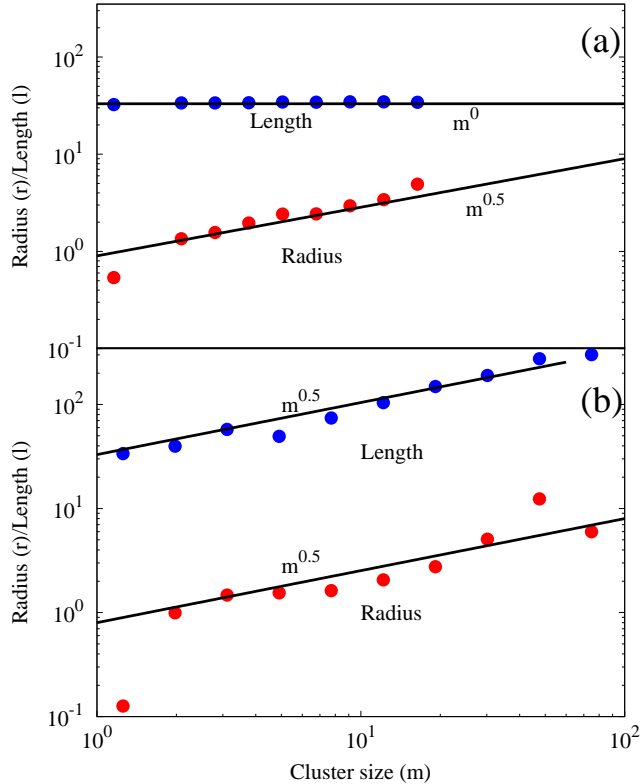


FIG. 4. The length and radius of different cluster sizes m for (a) $A = 2.01$ and (b) $A = 8.03$.

$\theta = 2/3$. This is in excellent agreement with the numerical value of 0.62 ± 0.07 from molecular simulations. When $A \gtrsim A_c$, the kernel is no longer homogeneous. For large m_1 and m_2 , it is homogeneous with $\lambda = -1/2$. Equation (8) gives $\theta = 2/3$. On the other hand, for small m_1, m_2 , we may ignore the dependence of radius on mass, and the kernel is homogeneous with $\lambda = -1$ or equivalently $\theta = 1/2$. The numerically obtained value of 0.62 ± 0.07 lies between these two bounds 0.5 and 0.67.

In our MD simulations, computational expense limits the number of PEs that can be studied to few hundreds. However, large-scale Monte Carlo simulations can be used to study the effect of the kernel for $A \gtrsim A_c$ on the measured θ . In these simulations, we start with $M = 10^5$ particles of mass 1. Any pair of particles of masses m_1 and m_2 undergo aggregation to form a particle of mass $m_1 + m_2$ with rate

$$K(m_1, m_2) = \Lambda(m_1^{-1} + m_2^{-1})(\sqrt{L^2 + m_1} + \sqrt{L^2 + m_2}), \quad (13)$$

where L is a parameter and Λ is chosen to be proportional to M^{-2} . The stochastic processes were simulated using standard Monte Carlo techniques. Each parameter value was averaged over 1000 histories. The results for $n(t)$ for different parameter values are shown in Fig. 5. As L increases the effective power law changes from -0.67 to -0.5 , and $\theta = 0.62 \pm 0.07$ from molecular dynamics falls within this range.

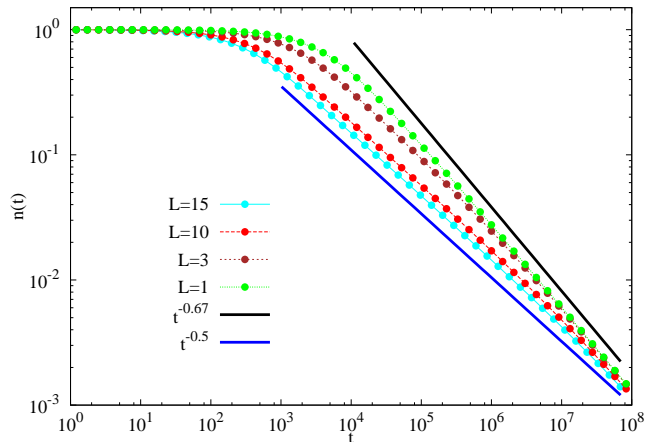


FIG. 5. Monte Carlo simulations with kernel as in Eq. (13) for different values of the parameter L .

From the above analysis based on Smoluchowski equation, we obtain $\theta = 2/3$ very similar to the value obtained through our MD simulations ($\theta = 0.62 \pm 0.07$). More accurate determination of θ through MD simulations will require much larger systems to be simulated for much longer times, currently a very expensive proposition. In earlier simulations of rigid PEs²³, it was suggested that the decay of the number of aggregates scales with time as t^{-1} different from the exponent obtained in this work ($t^{-0.62}$). This difference could be attributed to the assumption made in the analysis based on Smoluchowski equation in the earlier paper²³ that collisions occur between aggregates of approximately equal size⁵². In this work, we explicitly take into consideration collisions between aggregates of different sizes, which is much more realistic picture and hence we consider the result obtained in this work to be more accurate.

C. Two kinds of dynamics

For large values of A , we observed that the aggregates are collinear with the effective length increasing with size of aggregate[see Fig. 4(b)]. However, we find that such aggregates, when isolated, rearrange themselves from elongated to more compact cylindrical structures whose lengths are comparable to that of a single PE chain. To quantify this, we extract aggregates of size 3 and 10 from the simulations for $A = 8.03$ and with trivalent counterions, isolate them, and allow them to evolve for different values of A . A typical time profile of the end to end distance, R_{ee} is shown in Fig. 6(a). It decreases in steps with sudden decreases in length due to re-arrangement, separated in time. From the history averaged data (see Fig. 6), a relaxation time τ associated with the rearrangement may be extracted.

Thus, there are two time scales in the problem: one is the diffusion time scale corresponding to the time taken

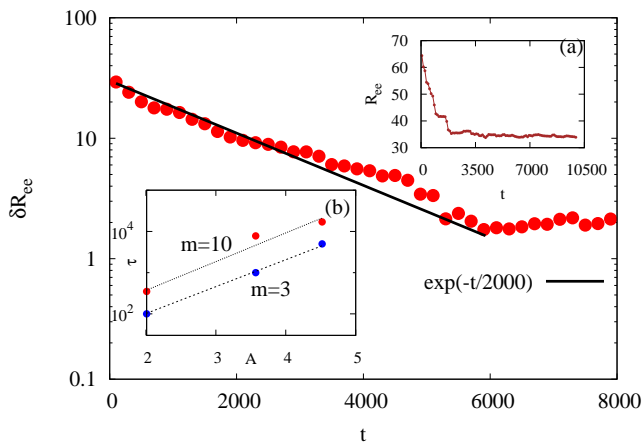


FIG. 6. The deviation of the end to end distance of the aggregate, δR_{ee} , from its equilibrium value as a function of time t . It decreases with time as an exponential. The data is for an aggregate of size three with trivalent counterions, $A = 3.57$ and averaged over three realizations. (a) The end to end distance R_{ee} for a single realization for the same parameters as in main plot. (b) The variation of the relaxation times τ with A for different aggregate sizes. The straight lines are $\exp(1.51A)$ ($m = 3$) and $\exp(1.61A)$ ($m = 10$).

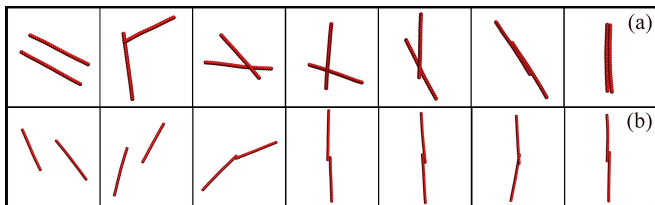


FIG. 7. Snapshots describing the merging of two PEs for (a) $A = 2.01$ (b) $A = 8.03$ for a system with trivalent counterions

for two aggregates to be transported nearby, and the second is the sliding time scale τ corresponding to the time taken for an aggregate to re-align itself into a compact cylindrical shape. The sliding time scale increases rapidly with A as seen in Fig. 6(b). For large A , the sliding time scale is much larger than the diffusion time scale and the re-alignment may be ignored.

We also find that the process by which two aggregates merge are different for small and large A . For small A , when two polyelectrolytes merge, they first orient in orthogonal directions, and the point of intersection moves towards the center. At later times, they align and rearrange themselves from elongated to more compact cylindrical structures [see Fig 7(a)]. For large A , the aggregates intersect and align themselves without sliding [see Fig. 7(b)].

IV. DISCUSSION AND CONCLUSION

In this paper, we studied the dynamics of aggregation of similarly-charged rigid PE chains using extensive MD simulations. It was shown that the dynamics of aggregation is effectively determined by short-ranged interactions between the PE chains, even though the monomers and counterions interact via long-ranged Coulomb interactions. We also showed that the number of aggregates decreases with time as a power law, $t^{-\theta}$, where the exponent θ is independent of the charge density of the PE chains, whether the counterions are divalent or trivalent, number density, and length of the PE chains. The data is modeled using Smoluchowski equation with coagulation kernel determined from the MD simulations. From the molecular dynamics simulations, we estimate $\theta = 0.62 \pm 0.07$, which is consistent with the value $\theta = 2/3$ obtained from the Smoluchowski equation.

The current simulations are only for systems with divalent and trivalent counterions. In an earlier paper⁴⁹, we had shown that monovalent counterions induce aggregation among similarly-charged PE chains, and preliminary data suggested $\theta \approx 0.66$. This, being consistent with the results obtained in this paper for divalent and trivalent counterions, we conclude that the dynamics is independent of valency of counterions. The charge density required for aggregation with monovalent counterions is much larger than that for divalent and trivalent counterions, resulting in much longer simulations needed for obtaining good data. For efficient computational purposes, we restrict the simulations in this paper to divalent and trivalent counterions.

In earlier simulations of rigid PE chains²³, by modeling the data with the Smoluchowski coagulation equation, it can be deduced that $\theta = 1$, different from $\theta \approx 2/3$ obtained in this paper. This difference could be attributed to the assumption made in the analysis of Ref.²³ that all aggregates are approximately of same size. In this paper, we explicitly take into consideration collisions between aggregates of different sizes, which is a much more realistic picture given the heterogeneous aggregate size distribution. In addition, the extensive MD simulations performed in this paper allow us to clearly distinguish between the exponents 1 and $2/3$, and hence we consider the result obtained in this paper to be more accurate.

It has been argued that for intermediate values of the charge density, finite size PE bundles exist at thermodynamic equilibrium, while further increase of charge density, results in phase separation and precipitation^{22,23,25,26}. However, in our simulations, for all the values of charge densities that we have considered, the number of aggregates decrease continuously as a power law, and shows no tendency to plateau which would be the case if finite sized bundles at thermodynamic equilibrium existed. In addition, we find that the cluster size distribution for different times obeys a simple scaling $N(m, t) \simeq t^{-2\theta} f(mt^{-\theta})$, where f is a scaling function (see Fig. 8), showing that the system continuously

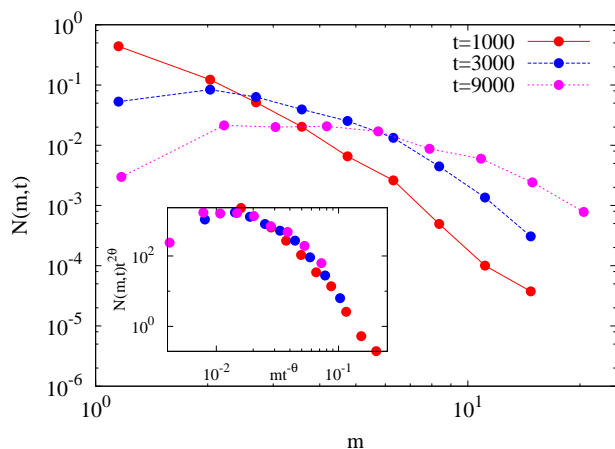


FIG. 8. Aggregate size distribution $N(m, t)$ for different times t for a system with trivalent counterions and $A = 2.01$. Inset: The data for different times collapse onto a single curve when m and $N(m, t)$ are scaled as shown in the figure with $\theta = 0.62$.

coarsens to presumably a phase separated state. This discrepancy in results could be due to the fact that the observation of finite sized bundles in Refs.^{22,23,25,26} was based on an arbitrarily chosen equilibration time.

It has also been suggested in many previous papers that similarly-charged rigid PE chains tend to approach each other at right angles, align and then slide to align with the bundle while merging with each other. This mode has been referred in the literature as zipper model^{22,23,26,61}. Another model of approach called collinear model was also proposed for rigid PE chains, in which the centers of mass of approaching PE chains lie on a line parallel to their longer axes⁶¹. This model was shown to have lower kinetic barrier of approach and can explain the observation of elongated structures in experiments^{62,63}. From our MD simulations, we see that the approach of merging depends significantly on the charge density of rigid PE chains. While zipper model seems to be the mode of aggregation for PE chains with lower charge density, the approach mechanism changes to collinear model for PE chains with high charge density.

All the simulations performed in this paper were in the absence of a solvent. From the obtained results, we expect that adding a solvent will result in modifying the dependence of diffusion constant on the aggregate size, and the results from the Smoluchowski equation should be carried forward. Likewise, adding salt will make the bare interactions even further short-ranged due to screening. This should not change the results except for modifying the critical charge density required for the onset of aggregation.

ACKNOWLEDGMENTS

We thank Upayan Baul for helpful discussions. The simulations were carried out on the supercomputing machines Annapurna, Nandadevi and Satpura at The Institute of Mathematical Sciences.

REFERENCES

- ¹V. A. Bloomfield, *Biopolymers* **31**, 1471 (1991).
- ²D. J. Needleman, M. A. Ojeda-Lopez, U. Raviv, H. P. Miller, L. Wilson, and C. R. Safinya, *Proceedings of the National Academy of Sciences of the United States of America* **101**, 16099 (2004).
- ³M. M. A. E. Claessens, C. Semmrich, L. Ramos, and A. R. Bausch, *Proceedings of the National Academy of Sciences* **105**, 8819 (2008).
- ⁴F. Huber, D. Strehle, and J. Kas, *Soft Matter* **8**, 931 (2012).
- ⁵S. Mohammadinejad, R. Golestanian, and H. Fazli, *Soft Matter* **8**, 3649 (2012).
- ⁶T. E. Angelini, H. Liang, W. Wriggers, and G. C. L. Wong, *Proceedings of the National Academy of Sciences* **100**, 8634 (2003), <http://www.pnas.org/content/100/15/8634.full.pdf>.
- ⁷D. A. Fletcher and R. D. Mullins, *Nature* **463**, 485 (2010).
- ⁸J. Stricker, T. Falzone, and M. L. Gardel, *Journal of Biomechanics* **43**, 9 (2010).
- ⁹P. H. J. Kouwer, M. Koepf, V. A. A. Le Sage, M. Jaspers, A. M. van Buul, Z. H. Eksteen-Akeroyd, T. Woltinge, E. Schwartz, H. J. Kitto, R. Hoogenboom, S. J. Picken, R. J. M. Nolte, E. Mendes, and A. E. Rowan, *Nature* **493**, 651 (2013).
- ¹⁰O. J. N. Bertrand, D. K. Fygenson, and O. A. Saleh, *Proceedings of the National Academy of Sciences* **109**, 17342 (2012).
- ¹¹P. A. Janmey, D. R. Slochower, Y.-H. Wang, Q. Wen, and A. Cebers, *Soft Matter* **10**, 1439 (2014).
- ¹²G. C. Wong and L. Pollack, *Annual Review of Physical Chemistry* **61**, 171 (2010).
- ¹³J. X. Tang, S. Wong, P. T. Tran, and P. A. Janmey, *Ber. Bunsenges. Phys. Chem.* **100**, 796 (1996).
- ¹⁴M. Sedláč and E. J. Amis, *J. Chem. Phys.* **96**, 817 (1992).
- ¹⁵J. J. Tanahatoc and M. E. Kuil, *J. Phys. Chem. B* **101**, 5905 (1997).
- ¹⁶R. Borsali, H. Nguyen, and R. Pecora, *Macromolecules* **31**, 1548 (1998).
- ¹⁷O. V. Zribi, H. Kyung, R. Golestanian, T. B. Liverpool, and G. C. L. Wong, *Phys. Rev. E* **73**, 031911 (2006).
- ¹⁸J. C. Butler, T. Angelini, J. X. Tang, and G. C. L. Wong, *Phys. Rev. Lett.* **91**, 028301 (2003).
- ¹⁹F. Bordi, C. Cametti, M. Diociaiuti, and S. Sennato, *Phys. Rev. E* **71**, 050401(R) (2005).
- ²⁰A. Muhrad, E. E. Grintsevich, and E. Reisler, *Biophysical Chemistry* **155**, 45 (2011).

- ²¹N. Huang, J. Tao, J. Liu, S. Wei, L. Li, and Z. Wu, *Soft matter* **10**, 4236 (2014).
- ²²H. Fazli and R. Golestanian, *J. Phys. : Condens. Matter* **21**, 424111 (2009).
- ²³H. Fazli and R. Golestanian, *Phys. Rev. E* **76**, 041801 (2007).
- ²⁴A. Savelyev and G. A. Papoian, *J. Am. Chem. Soc.* **129**, 660 (2007).
- ²⁵M. Sayar and C. Holm, *Euro. Phys. Lett.* **77**, 10601 (2007).
- ²⁶M. Sayar and C. Holm, *Phys. Rev. E* **82**, 031901 (2010).
- ²⁷M. J. Stevens, *Phys. Rev. Lett.* **82**, 101 (1999).
- ²⁸K. C. Lee, I. Borukhov, W. M. Gelbart, A. J. Liu, and M. J. Stevens, *Phys. Rev. Lett.* **93**, 128101 (2004).
- ²⁹S. Pietronave, L. Arcesi, C. D'Arrigo, and A. Perico, *J. Phys. Chem. B* **112**, 15991 (2008).
- ³⁰N. G. Jensen, R. J. Mashl, R. F. Bruinsma, and W. M. Gelbart, *Phys. Rev. Lett.* **78**, 2477 (1997).
- ³¹B. Luan and A. Aksimentiev, *J. Am. Chem. Soc.* **130**, 15754 (2008).
- ³²R. Bruinsma, *Phys. Rev. E* **63**, 061705 (2001).
- ³³A. Diehl, H. A. Carmona, and Y. Levin, *Phys. Rev. E* **64**, 011804 (2001).
- ³⁴J. O. Ray and G. S. Manning, *Macromolecules* **33**, 2901 (2000).
- ³⁵A. Perico and A. Rapallo, *J. Chem. Phys.* **134**, 055108 (2011).
- ³⁶S. Zhou, *Langmuir*, *Langmuir* **29**, 12490 (2013).
- ³⁷A. V. Ermoshkin and M. O. de la Cruz, *Phys. Rev. Lett.* **90**, 125504 (2003).
- ³⁸C. Broedersz and F. MacKintosh, *Rev. Mod. Phys.* **86**, 995 (2014).
- ³⁹G. S. Manning, *Eur. Phys. J. E* **34**, 132 (2011).
- ⁴⁰A. Yethiraj, *Phys. Rev. Lett.* **78**, 3789 (1997).
- ⁴¹A. Yethiraj, *The Journal of Physical Chemistry B* **113**, 1539 (2009).
- ⁴²G. S. Manning, *Soft matter* **10**, 3738 (2014).
- ⁴³B. D. Ermi and E. J. Amis, *Macromolecules* **31**, 7378 (1998).
- ⁴⁴Y. Zhang, J. F. Douglas, B. D. Ermi, and E. J. Amis, *J. Chem. Phys.* **114**, 3299 (2001).
- ⁴⁵J. J. Arenzon, J. F. Stilck, and Y. Levin, *Eur. Phys. J. B* **12**, 79 (1999).
- ⁴⁶J. J. Arenzon, Y. Levin, and J. F. Stilck, *Physica A* **283**, 1 (2000).
- ⁴⁷F. J. Solis and M. O. de la Cruz, *Phys. Rev. E* **60**, 4496 (1999).
- ⁴⁸E. Allahyarov, G. Gompper, and H. Löwen, *Phys. Rev. E* **69**, 041904 (2004).
- ⁴⁹A. Varghese, R. Rajesh, and S. Vemparala, *The Journal of Chemical Physics* **137**, 234901 (2012).
- ⁵⁰A. Varghese, S. Vemparala, and R. Rajesh, *J. Chem. Phys.* **135**, 154902 (2011).
- ⁵¹M. V. Smoluchowski, *Z. Phys. Chem.* **92** (1917).
- ⁵²W. B. Russel, D. A. Saville, and W. R. Schowalter, *Colloidal Dispersions* (Cambridge University Press, Cambridge, 1989).
- ⁵³See <http://lammmps.sandia.gov> for details about the package.
- ⁵⁴S. J. Plimpton, *J. Comp. Phys.* **117**, 1 (1995).
- ⁵⁵S. Nosé, *J. Chem. Phys.* **51**, 511 (1984).
- ⁵⁶W. G. Hoover, *Phys. Rev. A* **31**, 1695 (1985).
- ⁵⁷R. W. Hockney and J. W. Eastwood, *Computer Simulations Using Particles* (McGraw-Hill, New York, 1975).
- ⁵⁸F. Leyvraz, *Physics Reports* **383**, 95 (2003).
- ⁵⁹C. Connaughton, R. Rajesh, and O. Zaboronski, in *Handbook of Nanophysics: Clusters and Fullerenes*, edited by K. D. Sattler (Taylor and Francis, 2010).
- ⁶⁰P. L. Krapivsky, S. Redner, and E. Ben-Naim, *A kinetic view of statistical physics* (Cambridge University Press, 2010).
- ⁶¹T. T. Nguyen and B. I. Shklovskii, *Phys. Rev. E* **65**, 031409 (2002).
- ⁶²F. Bordi, C. Cametti, S. Sennato, and M. Diociaiuti, *Biophysical Journal* **91**, 1513 (2006).
- ⁶³M. Susoff, D. Winter, C. D. Eisenbach, and W. Oppermann, *The Journal of Physical Chemistry B* **112**, 4519 (2008).